Cancer Letters 442 (2019) 341–350

Contents lists available at ScienceDirect

Cancer Letters

journal homepage: www.elsevier.com/locate/canlet

Original Articles

RITA downregulates Hedgehog-GLI in medulloblastoma and rhabdomyosarcoma via JNK-dependent but p53-independent mechanism

Ani Azatyan[a], Gabriel Gallo-Oller[b,1], Yumei Diao[a,1], Galina Selivanova[c], John Inge Johnsen[b], Peter G. Zaphiropoulos[a,*]

[a] Department of Biosciences and Nutrition, Karolinska Institutet, Huddinge, Sweden
[b] Department of Women's and Children's Health, Childhood Cancer Research Unit, Karolinska Institutet, Stockholm, Sweden
[c] Department of Microbiology, Tumor and Cell Biology, Karolinska Institutet, Stockholm, Sweden

ARTICLE INFO

Keywords:
Hedgehog signaling
GLI1 oncogene
Small molecule inhibitor
Mouse xenograft
RNA-sequencing

ABSTRACT

Overactivation of the Hedgehog (HH) signaling pathway is implicated in many cancers. In this study, we demonstrate that the small molecule RITA, a p53 activator, effectively downregulates HH signaling in human medulloblastoma and rhabdomyosarcoma cells irrespective of p53. This is mediated by a ROS-independent activation of the MAP kinase JNK. We also show that *in vitro* RITA sensitized cells to the GLI antagonist GANT61, as co-administration of the two drugs had more pronounced effects on cell proliferation and apoptosis. *In vivo* administration of RITA or GANT61 suppressed rhabdomyosarcoma xenograft growth in nude mice; however, co-administration did not further enhance tumor suppression, even though cell proliferation was decreased. RITA was more potent than GANT61 in downregulating HH target gene expression; surprisingly, this suppressive effect was almost completely eliminated when the two drugs were administered together. Notably, RNA-seq demonstrated a broader response of pathways involved in cancer cell growth in the combination treatment, providing a plausible interpretation for tumor reduction in the absence of HH signaling downregulation.

1. Introduction

HH-GLI signaling is one of the major pathways involved in both normal and neoplastic development [1–4]. Inappropriate activation of this pathway has been linked to cancer, including medulloblastoma, rhabdomyosarcoma, basal cell carcinoma and cancers of the lung, stomach, pancreas, colon and prostate [5,6]. Medulloblastoma (MB) and rhabdomyosarcoma (RMS) are heterogeneous and aggressive classes of childhood tumors. Subtypes of both MB (Sonic HH (SHH)) [7] and HH-linked RMS tumors [4,8,9] have been characterized with abnormally activated HH signaling. Importantly, both SHH MB and RMS tumors often harbor recurrent mutations in the p53 gene, and a p53-null background dramatically enhances tumorigenesis in mouse models [10,11]. Consequently, in these tumors, in addition to targeting HH signaling, therapeutic strategies aiming at reactivating p53 may have certain advantages.

In mammals, the canonical HH signaling pathway is initiated by extracellular HH ligands binding to Patched (PTCH1, PTCH2) [4,12]. This releases the PTCH1 inhibitory effects on the signaling molecule Smoothened (SMO), facilitating downstream activation of the Glioma-associated oncogenes (GLI1, GLI2, GLI3) family of Zn-finger transcription factors. Upon activation, the GLI factors translocate to the nucleus and promote transcription of HH target genes [2,3,12,13]. While GLI1 acts as an activator of the pathway, amplifying the HH signal, GLI2 and especially GLI3 have both activator and repressor functions. Notably, effective inhibition of the GLIs can represent a promising treatment option for HH-activated cancers.

Studies on the small molecule inhibitor of GLI1/2, GANT61 (GLI antagonist 61) have proven its efficacy in suppressing HH signaling-dependent cancer cell growth *in vitro* and *in vivo* [14], including RMS [15], neuroblastoma [16], pancreas [17], small cell lung [18] and hepatocellular cancers [19]. Another small molecule, NSC652287 [20], later named RITA (reactivation of p53 and induction of tumor cell apoptosis) was identified as a potential tumor suppressor. In early studies RITA was proposed to exert its effects in a p53-dependent manner through activation of both mutant and wild-type p53, resulting in tumor cell growth inhibition and p53-dependent apoptosis *in vitro* and *in vivo* [21–24]. However, several recent studies suggest p53-independent effects of RITA, questioning its selective binding to p53 [25], and even suggesting that p53 might be dispensable for RITA activity, as

* Corresponding author.
E-mail address: peter.zaphiropoulos@ki.se (P.G. Zaphiropoulos).
[1] Equal contribution.

https://doi.org/10.1016/j.canlet.2018.11.005
Received 20 July 2018; Received in revised form 26 October 2018; Accepted 5 November 2018

Abbreviations

BCL2	B-cell lymphoma 2
BP	Biological processes
CC	Cell components
DCFDA	2,7-dichlorofluorescin diacetate
DXR	Doxorubicin
EdU	5-ethynyl-2-deoxyuridine
EGO	Enrichment gene ontology
GANT61	GLI antagonist 61
GO	Gene ontology
GLI	Glioma-associated oncogene
HH	Hedgehog
IGF1R	Insulin-like growth factor 1
KEGG	Kyoto encyclopedia of genes and genomes
MAPK	Mitogen-activated protein kinase
MB	Medulloblastoma
MEF	Mouse embryonic fibroblast
MF	Molecular functions
NAC	N-acetyl-L-cysteine
NOXA	PMAIP1/Phorbol-12-myristate-13-acetate-induced protein 1
OXP	Oxaliplatin
PIKCA	Phospatidylinositol-4,5-bisphosphate 3-kinase catalytic subunit alpha
PI3K/Akt	Phosphatidylinositol 3-kinase/Aktivating receptor tyrosine kinase
PTCH	Patched
RITA	Reactivation of p53 and induction of tumor cell apoptosis
RMS	Rhabdomyosarcoma
ROS	Reactive oxygen species
RPLP0	Ribosomal protein lateral stalk subunit P0
SAPK/JNK	Stress-activated protein kinase/Jun amino-terminal kinase
SHH	Sonic Hedgehog
siRNA	Small-interfering RNA
SMO	Smoothened
TBP	TATA-binding protein
TBHP	Tert-butyl hydroperoxide
TGF-beta	Transforming growth factor-beta
TrxR1	Thioredoxin reductase 1
WST-1	Watersoluble tetrazolium salt 1

its effects are largely mediated through induction of DNA damage [26], irrespective of the cell's p53 status [27]. Additionally, it was demonstrated that whereas p53 has a central role for RITA-mediated effects in wild-type cells, neither p53, nor the other two homologs of p53 (p63 or p73) are essential for the RITA response in mutant or p53 null cells [28]. Notably, RITA-induced apoptosis is predominantly mediated by the Stress-activated protein kinase/Jun amino-terminal kinase (SAPK/JNK) and p38 Mitogen-activated protein kinase (MAPK) pathways [28,29], which are known to be activated in response to a wide range of extra- and intra-cellular stress stimuli [30]. Other studies have demonstrated reactive oxygen species (ROS)-dependent JNK activation as a possible mode of RITA action [28], which can induce DNA damage, with RITA interacting and inhibiting Thioredoxin reductase 1 (TrxR1), leading to further ROS induction [31,32]. In addition, the JNK pathway has been linked to HH signaling and several studies have indicated interactions between phospho-JNK (activated form) and GLI proteins [33–36]. These studies provide an appealing hint on the mechanism of a possible RITA - > JNK - > HH-GLI axis.

In the present study, we focused on tumor cell lines of distinct origin and p53 background, the Rh36 RMS cells with wild-type p53 and the Daoy MB cells carrying a homozygous cysteine to phenylalanine mutation in codon 242 of the TP53 gene [37,38]. We found that RITA can effectively downregulate HH signaling in these cell lines irrespective of siRNA mediated p53 depletion. Moreover, siRNA depletion of the upstream activator of canonical HH signaling SMO did not abrogate the response of HH target genes to RITA treatment, suggesting that RITA acts downstream of SMO. Remarkably, RITA was capable to reduce HH signaling activity even in the context of HH pathway activation by SAG treatment or GLI1 overexpression. In addition, we demonstrated that this downregulation of HH signaling is mediated by ROS-independent activation of JNK kinase, since inhibition of JNK but not of ROS accumulation fully reverted RITA's impact on HH target genes. Furthermore, the cytotoxic effects of RITA were quite distinct compared to the widely used DNA damaging agents doxorubicin and oxaliplatin. Surprisingly, although RITA and GANT61 co-administration enhanced the effects of each drug on cell proliferation and apoptosis, there was a similar reduction of tumor growth in mouse Rh36 xenografts following RITA, GANT61 or combinatorial treatment. Finally, compared to single treatment, co-administration of the drugs resulted in a more stable reduction of tumor volume, reduced tumor cell proliferation and was associated with an expanded spectrum of GO terms and KEGG pathways involved in cellular growth.

2. Materials and methods

2.1. Cell culture and reagents

The Daoy MB cell line, the Rh36 embryonal RMS cell line, the MCF7 breast cancer cell line and the MEF Ptch1$^{-/-}$ and Sufu$^{-/-}$ derived cell lines, where the negative regulators of HH signaling Ptch1 and Sufu, are eliminated, have been used previously [39–41]. Cell lines were assessed for mycoplasma contamination (#LT07-218, Lonza, MycoAlert™ mycoplasma detection kit, Switzerland). Briefly, Daoy, Ptch1$^{-/-}$ and Sufu$^{-/-}$ cells were cultured in EMEM medium with L-glutamine (Lonza, Switzerland) and 10% fetal bovine serum (FBS) (Sigma-Aldrich, USA), Rh36 cells in RPMI-1640 medium with L-glutamine (Gibco, USA) and 10% FBS and MCF7 cells in DMEM (Sigma-Aldrich, USA) with 10% FBS. All media were supplemented with 100 IU/ml penicillin/streptomycin (Sigma-Aldrich, USA) and maintained in a 5% CO_2 humidified incubator at 37 °C.

2.2. Drug treatments

RITA was purchased from Santa Cruz Biotechnology (#sc-202753, USA) or obtained from NCI (USA), GANT61 was a kind gift of Rune Toftgård (Karolinska Institutet, Stockholm, Sweden), doxorubicin (DXR, #D1515), oxaliplatin (OXP, #O9512), JNK inhibitor (JNKI, #SP600125), resveratrol (#R5010), N-acetyl-L-cysteine (NAC, #S5567) and nutlin-3a (#N6287) were purchased from Sigma-Aldrich (USA), APR-246 (PRIMA-1Met) was provided by Aprea AB (Sweden) and Smoothened agonist (SAG, #566660) was purchased from Merck (Germany). Working solutions of RITA, GANT61, DXR, resveratrol, SP6001125 and SAG were diluted in DMSO, OXP was diluted in double distilled water (WST-1 assay) or DMSO (qPCR assay), NAC in double distilled water. For resveratrol and NAC treatments, only fresh-made working solutions (from powder) were used. For SAG treatments, Daoy cells were starved in OPTIMEM (Gibco, USA) medium for 24hr and treated with indicated drug mixtures in EMEM medium with L-glutamine (Lonza, Switzerland) and 0.5% FBS (Sigma-Aldrich, USA).

2.3. siRNA and plasmid transfections

siRNAs targeting human p53 (#sc-29435, Santa Cruz Biotechnology, USA), p63, p73 (Sigma-Aldrich, USA) [Supplementary Table 1], SMO (#sc-40161, Santa Cruz Biotechnology, USA) and

control siRNAs (#SIC001, Sigma-Aldrich, USA) were used. For plasmid transfections, the pGLI1 expression construct [39] and a control pCMV plasmid were used. Cells were plated in 6-well plates at ≈50–70% confluency and transfected with 50 nM siRNA or 1500–2500 ng plasmids for 24hr when ≈80% confluent. Lipofectamine RNAiMAX transfection reagent (Invitrogen, USA) was used for siRNA, and Lipofectamin LTX with Plus™ reagent (Invitrogen, USA) for plasmid transfections according to the manufacturer's instructions.

2.4. RNA isolation, cDNA synthesis and real-time qPCR

Total RNA from cell lines or tumor tissue samples was isolated with E.Z.N.A. total RNA kit I (#R6834-02, Omega Bio-tek, USA) according to the manufacturer's instructions. For RNA isolation from tumor samples, small pieces of tumors (20–40 mg in 700 µL TRK lysis buffer) were homogenized by Qiagen TissueRuptor (Germany) and proceeded further according to the manufacturer's instructions. The RNA was quantified spectrophotometrically with an Infinite 200 NanoQuant microplate reader (TECAN, Switzerland), and 1000 ng of RNA was used for cDNA synthesis. cDNA were generated with Superscript III (Invitrogen, USA), random N6 primers (NEB, USA) and RNAase inhibitor (NEB, USA). Real-time qPCR was performed using FastStart Universal SYBR Green Master (Rox) (Roche, Switzerland) on a 7500 fast real-time PCR system (Applied Biosystems, USA), with primers to detect human GLI1, PTCH1, PTCH2, SMO, HHIP, p53, BCL2, IGF1R, PIKCA, NOXA, and murine Gli1, Gli2, Ptch1, Ptch2, Hhip [Supplementary Table 1]. The primers were designed spanning 2 adjacent exons or exon junctions to avoid genomic DNA amplification using the NCBI primer blast tool. All amplifications were run in triplicate and the fold change was normalized to the expression of human TBP and/or RPLP0 or murine Gapdh housekeeping genes. All qPCR reactions were performed under the following conditions: 95 °C for 10min, followed by 40 cycles of 95 °C for 10sec, 65 °C for 30sec. The relative expression was determined with the $2^{-\Delta\Delta Ct}$ method [42], by subtracting the Ct value of the housekeeping gene(s) from the Ct value of the interrogated transcripts (ΔCt), and normalized to the ΔCt values obtained with the control treatment. Reverse transcriptase negative controls for each primer pair were run to ensure no DNA contamination.

2.5. Cell proliferation assay

Cells were plated in 6-well plates at 50% confluency and treated with RITA and/or GANT61 for 48hr (Daoy) or 24hr (Rh36) when 60% confluent, followed by 3hr (Daoy) or 4.5hr (Rh36) of 10 µM EdU (5-ethynyl-2-deoxyuridine, Invitrogen, USA) incubation. As a negative control, the cells were treated with DMSO alone. EdU incorporation was detected by fluorescent-azide coupling reaction according to the manufacturer's instructions (#C10425, Click-iT EdU Alexa Fluor® 488 Flow Cytometry kit, Invitrogen, USA). For each treatment, 10000–20000 cells were analyzed on a FACS Calibur machine (BD Biosciences, USA). Cell cycle distribution was calculated using the CellQuest software (BD Biosciences, USA) to determine the percentage of cells at the S-phase. Gating was performed to eliminate aggregated cells and cell debris. Non-EdU stained cells were used to set the plot area for the EdU treated cells.

2.6. Cell viability assay

3.5×10^4 (Daoy) or 4.5×10^4 (Rh36) cells were seeded in 96-well plates and left to grow for 24hr until 80% confluent. Cells were treated with RITA, DXR and OXP for 48hr (Daoy) or 24hr (Rh36). Metabolic activity was measured with the WST-1 (Water soluble tetrazolium salt 1) reagent (Roche, Switzerland) according to the manufacturer's instructions, and the number of viable cells was quantified at 450 nm, with reference wavelength of 690 nm (Infinite M200 PRO, TECAN, Switzerland). Each measurement was represented as the mean of technical triplicates.

2.7. Western blot

Cells were lysed with RIPA buffer (150 mM NaCl, 50 mM Tris base pH 8.0, 1 mM EDTA, 0.5% sodium deoxycholate, 1% DTT, 1 mM PMSF, and 1 mM Na_3VO_4) supplemented with Complete protease inhibitor tablets (Roche, Switzerland) and Phosphatase inhibitor cocktail 1 (Sigma-Aldrich, USA). Proteins were separated by 7.5% sodium dodecyl sulfate polyacrylamide gel electrophoresis (PAGE) followed by transfer (230 mA for 1hr) to an Immobilon-PVDF membrane (Millipore, USA). The membrane was incubated at 4 °C overnight in the StartingBlock™ T20 (TBS) Blocking buffer (#337453, Thermo Scientific, USA) with primary antibodies against p53 (FL-393, #sc-6243, Santa Cruz Biotechnology, 1:10000), GLI1 (#2553, Cell Signaling, 1:500), SMO (#sc-166685, Santa Cruz Biotechnology, 1:1000), Vinculin (hVIN-1, #V9131, Sigma-Aldrich, 1:10000), Phospho-SAMPK/JNK (#9255, Cell Signaling, 1:1000), β-actin (#A5441, Sigma-Aldrich, 1:5000), followed by anti-rabbit or anti-mouse secondary antibodies incubation for 1hr in StartingBlock™ T20 (TBS) and visualized using Pierce ECL chemiluminescent substrate (Thermo Scientific, USA).

2.8. In vivo studies with the Rh36 cell xenograft tumor model

3×10^6 Rh36 cells in suspension were mixed with equal volume (1/1 ratio) of Matrigel (#356234, Corning, USA) and were injected subcutaneously into the right flank of immunodeficient nude mice (female 5–6 week old, NMRI-*nu/nu*, Scanbur, Denmark), n = 44. At palpable xenograft tumor size, volume ≥0.150 mL, animals were randomized to receive RITA (dissolved in 100% DMSO and administered by intraperitoneal injection at a dose of 10 mg/kg in 100–140 µL PBS solution), GANT61 (dissolved in 70% ethanol and administered by oral gavage feeding at a dose of 75 mg/kg in 200–300 µL glucose solution), combination treatment of 10 mg/kg RITA (intraperitoneal injection) and 75 mg/kg GANT61 (oral gavage feeding) or no treatment (control). Tumors were measured daily and tumor volume was calculated as V = (tumor width)^2 x (tumor length) x 0.44. In this study, mice received daily treatments of RITA or/and GANT61 for 20 consecutive days and then sacrificed.

The animals were maintained at a maximum of 6 per cage and given sterile water and food at libitum, monitored for signs of toxicity, including weight loss inspection every day. No signs of toxicity or weight loss were detected during this study. At sacrifice, tumors were extracted, photographed, weighted and dissected into smaller parts. Half of the tumor was snap-frozen in liquid nitrogen and the other half fixed in formaldehyde for further analyses. Animal experiments were approved by regional ethics committee for animal research (N231/14), appointed and under the control of the Swedish Board of Agriculture and the Swedish Court. The animal experiments presented here were in accordance with the national regulations and animal care was in accordance with the Karolinska Institutet guidelines (SFS 1988:534, SFS 1988:539, and SFS 1988:541).

2.9. Illumina RNA sequencing

4 tumor samples were selected from each treatment group (16 samples in total), and aliquots of total RNA extracted from each sample (as described in “RNA isolation, cDNA synthesis and real-time qPCR” section) were assessed for total RNA integrity with RNA ScreenTape System (G2964AA, Agilent Technologies, USA) using the TapeStation 2200 (Agilent Technologies, USA). ≈100 ng of total RNA was used to generate stranded mRNA libraries with the TruSeq® Stranded mRNA Low Throughput Sample Preparation kit according to manufacturer's instructions (#15031047, Illumina, USA). The concentration and quality of the cDNA libraries were assessed by Qubit (Life Technologies, USA) and TapeStation, respectively. The cDNA libraries were

normalized and pooled for sequencing on the Illumina NextSeq 550 platform using the Illumina NextSeq 500/550 High Output v2 kit (75 cycles; single-read). The description of bioinformatical analyses is given in the Supplementary materials and methods section: Illumina RNA sequencing.

2.10. Statistical analyses

In vitro assays were performed independently at least three times and *in vivo* assays were carried out with n = 7–9 mice. The results are represented as a mean value ± standard error of the mean. Once general assumptions of specific statistical tests were assessed, a parametric or nonparametric analysis was applied. Comparisons between two groups were analyzed by *t*-test. Comparisons between three or more groups were analyzed by multiple *t*-test or analysis of variance (ANOVA). Detailed descriptions of statistical analyses are given in Figure legends. Significance levels (at least $p < 0.05$) were set as indicated in the Figure legends. Statistical analyses were performed using GraphPadPrism v7.0d, except for RNA-seq data analyses, which was performed using R software (R-v3.4.3 and R-Studio-v1.0.143). More detailed descriptions of statistical analyses and softwares are given in respective sections of Figure legends and Supplementary materials and methods.

3. Results

3.1. RITA downregulates HH signaling target gene expression irrespective of p53

To explore the effect of RITA on HH signaling, three tumor cell lines, the RMS Rh36 and the breast cancer MCF7 cells, which harbor wild-type p53, and their proliferation depends on the terminal effector of HH signaling, the GLI1 transcription factor [15,41] and the MB Daoy cells, which harbor mutant p53 and are responsive to HH signaling activation [40], were analyzed. Treatment of these cells with 1 μM RITA downregulated the RNA expression of typical HH signaling target genes, e.g. GLI1, GLI2, PTCH1, PTCH2, irrespective of p53 depletion with siRNAs [Fig. 1A and B; Figs. S1A and B]. Remarkably, in Daoy cells 1 μM RITA was capable of reducing HH signaling target genes (GLI1, HHIP, PTCH1, PTCH2) in the context of activation of HH signaling by the Smoothened agonist (SAG) [Fig. 1C]. In addition, in GLI1-transfected Daoy cells 1 μM RITA, again, elicited detectable reduction of PTCH1 and PTCH2 gene expression [Fig. 1D].

Moreover, to address whether RITA affects HH signaling via the canonical, SMO-dependent pathway, Daoy, Rh36 and MCF7 cells were also treated with siRNAs targeting SMO. Depletion of SMO did not confer major changes in the observed response, implying that RITA may act downstream of SMO [Fig. 1A; Fig. S1A and B]. It is noteworthy that in the Daoy cell line RITA elicited only a small increase in the expression of NOXA out of the p53 target genes analyzed [Fig. 1A; Fig. 2A and B; Fig. 3A]. Moreover, this occurred even when p53 was depleted [Fig. 1A], arguing that the observed NOXA response is not dependent on p53. These observations suggest that RITA can not elicit a typical p53-dependent response in the mutant p53 cells analyzed. In line with this is the inability of RITA to increase p53 protein levels in this cellular context [Fig. 1B]. Noteworthy is that the RITA downregulation of HH signaling is also mostly independent of the two other p53 homologs, p63 and p73, as siRNA depletion of neither p63 nor p73 consistently affected the response to RITA treatment [Figs. S1C and D].

Interestingly, over a wide range of concentrations (0.5μM-20μM),

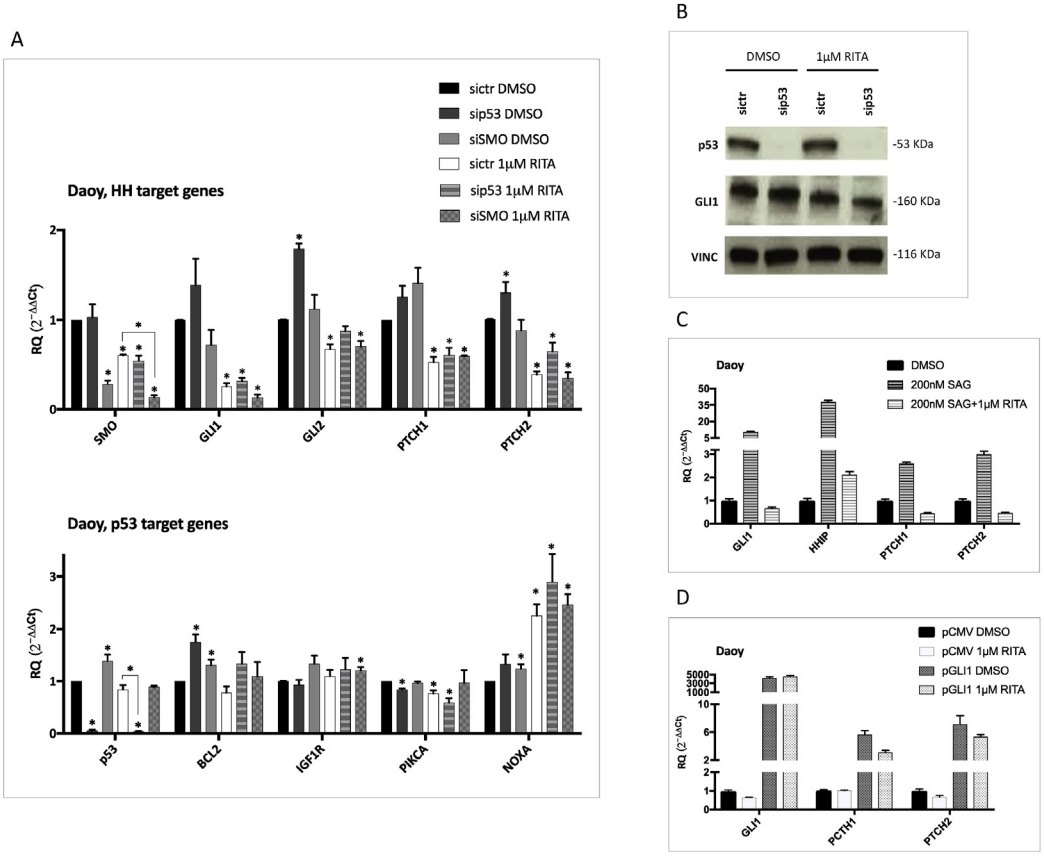

Fig. 1. RITA suppresses HH signaling in Daoy cells irrespective of p53 depletion. Daoy cells were transfected with siRNAs against SMO, p53 and control siRNAs (sictr) for 24hr, followed by 48hr 1 μM RITA or DMSO treatment. RNA expression of **(A)** HH and p53 target genes is presented as relative expression ($2^{-\Delta\Delta Ct}$ values), normalized to the housekeeping genes (TBP and RPLP0) and the control treatment (sictr and DMSO treated cells). Error bars indicate the SEM of three independent biological replicates. RQ denotes the relative quantification of the mRNA expression. Multiple *t*-test using Holm-Sidak's method (p values computed while not assuming consistent SD) was applied to calculate statistically significant differences (*:$p < 0.05$) between each treatment vs. the control (sictr and DMSO treated cells), highlighting the effectiveness of siRNA treatment. **(B)** Protein levels of p53 and GLI1 were analyzed by Western blot. Vinculin (VINC) was used as an endogenous protein control. **(C, D)** Daoy cells were co-treated with 200 nM Smoothened agonist (SAG) and 1 μM RITA for 72hr (C) or transfected with 2.5 μg pGLI1 or pCMV expression plasmids for 6hr, followed by 24hr RITA or DMSO treatment (D). RNA expression of HH target genes is presented as relative expression ($2^{-\Delta\Delta Ct}$ values), normalized to the housekeeping gene (TBP) and the control treatment (DMSO (C); pCMV and DMSO (D)). Representative experiments of three independent biological replicates are shown; error bars indicate SD of three technical replicates. The GLI1 levels in columns three and four of panel D reflect efficiency of pGLI1 plasmid transfection. Note that RITA reduces HH signaling target gene expression both in the context of basal and activated levels of the HH pathway, the latter induced by SAG treatment or GLI1 overexpression.

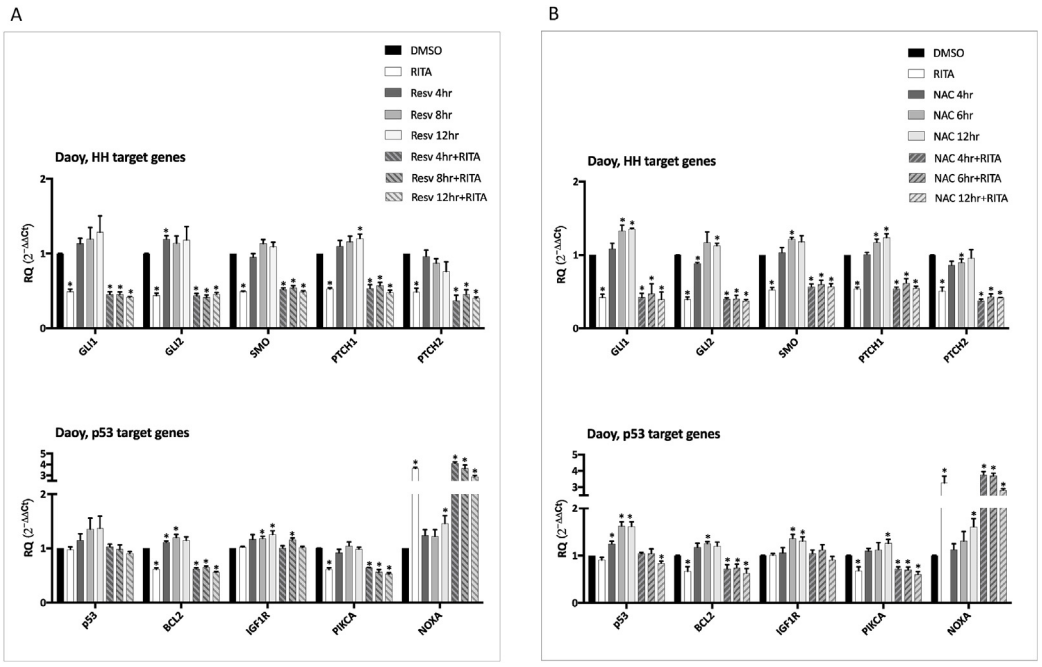

Fig. 2. Treatment with the ROS scavengers resveratrol and NAC does not rescue RITA-induced HH signaling downregulation. Daoy cells were pre-treated with 1 μM resveratrol (Resv) for 4, 8 or 12hr (**A**) and 5 mM NAC for 4, 6 or 12hr (**B**), followed by 1 μM RITA treatment for 48hr. RNA expression of HH and p53 target genes are presented as relative expression ($2^{-\Delta\Delta Ct}$ values), normalized to the housekeeping gene TBP and the control treatment (DMSO treated Daoy cells). Error bars indicate the SEM of three independent biological replicates. RQ denotes the relative quantification of the mRNA expression. Multiple *t*-test using Holm-Sidak's method (p values computed while not assuming consistent SD) was applied to determine statistically significant differences (*:$p < 0.05$) between each treatment vs. the DMSO control. Note that the suppressive effects of RITA on HH signaling do not depend on ROS activation.

RITA was not able to downregulate HH signaling in Sufu$^{-/-}$ or Ptch1$^{-/-}$ MEFs, with activated HH signaling [Figs. S1E and F], with only 20 μM RITA eliciting a detectable reduction in the Ptch1$^{-/-}$ MEFs [Fig. S1F].

Together, these data suggest that the RITA-mediated downregulation of HH signaling is p53-independent.

3.2. The effect of RITA on HH signaling is independent of ROS activation

It has previously been suggested that RITA contributes to ROS accumulation and ROS-induced cell apoptosis [31,32]. To test the involvement of such mechanisms in the observed HH signaling downregulation, we examined the impact of the ROS scavengers resveratrol and NAC on the RITA effects in Daoy [Fig. 2; Figs. S2C and D; Figs. S3A and B] and Rh36 [Figs. S2A,B,E,F; Figs. S3A and B] cells. Surprisingly, we found that 4, 8 and 12hr 1 μM resveratrol or 5 mM NAC pre-treatments of Daoy [Fig. 2A and B] and Rh36 [Figs. S2A and B] cells prior to the 48hr RITA administration did not rescue the RITA effects on HH targets gene expression. Moreover, the RITA effects on p53 targets were also largely unchanged. Additionally, these results were further validated by resveratrol or NAC co-treatments with 1 μM RITA for both Daoy [Figs. S2C and D] and Rh36 [Figs. S2E and F] cells.

In Rh36 cells, the p53 target genes show stronger response to RITA treatment than in Daoy cells, reflecting p53 activation. Resveratrol

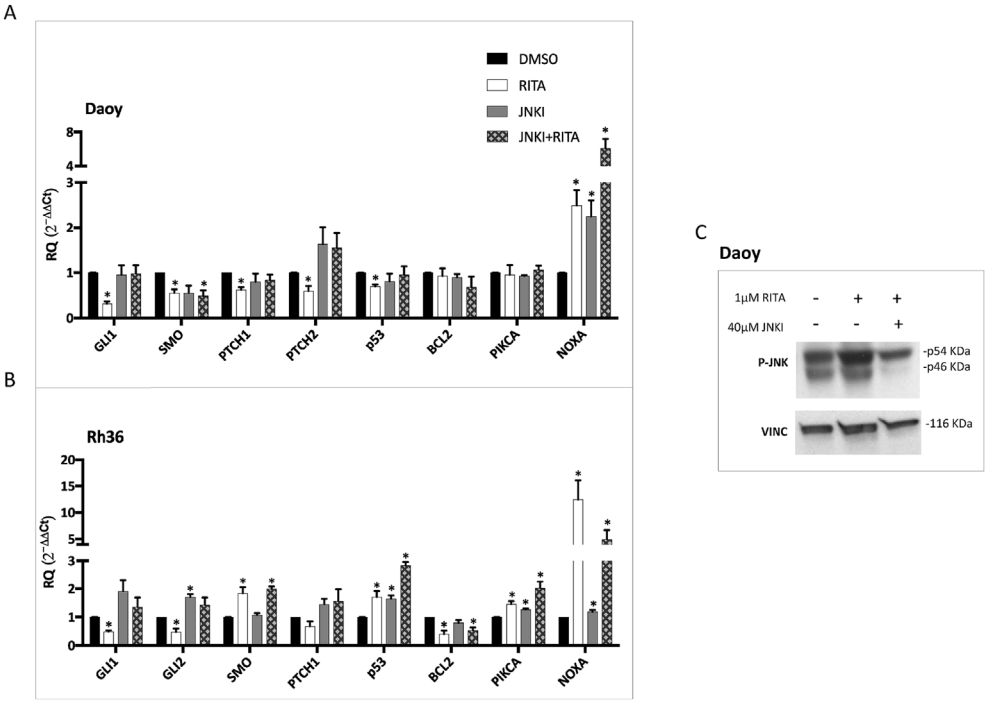

Fig. 3. Inhibition of JNK activity blocks the RITA-induced effects on HH signaling. **(A)** Daoy and **(B)** Rh36 cells were co-treated with 1 μM RITA and 40 μM JNK inhibitor SP600125 (JNKI) for 48 (Daoy) or 24 (Rh36) hr. RNA expression of HH and p53 target genes are presented as relative expression ($2^{-\Delta\Delta Ct}$ values), normalized to the housekeeping gene (TBP) and the control treatment (DMSO treated Daoy or Rh36 cells respectively). Error bars indicate the SEM of three independent biological replicates. RQ denotes the relative quantification of the mRNA expression. Multiple *t*-test using Holm-Sidak's method (p values computed while not assuming consistent SD) was applied to determine statistically significant differences (*:$p < 0.05$) between each treatment vs. the DMSO control. Note that the suppressive effects of RITA on Hedgehog signaling are abrogated by JNK inhibition. **(C)** Daoy cells were treated with 1 μM RITA and 40 μM JNKI for 48hr. Protein levels of phosphorylated JNK (P-JNK) were analyzed by Western blot. Vinculin (VINC) was used as an endogenous protein control. Note the increased signal of the 54 KDa (p54) and 46 KDa (p46) JNK isoforms following RITA treatment, which is reduced by JNKI co-treatment.

[Figs. S2A,C,E] or NAC [Figs. S2B,D,F] were not capable to revert this response, indicating that p53 target gene induction is not due to ROS [31].

This ineffectiveness of resveratrol and NAC demonstrates that the impact of RITA on HH signaling, in the context of Daoy and Rh36 cells, does not depend on ROS activation.

3.3. The inhibitory effect of RITA on HH signaling is mediated by JNK kinase

To further examine the mechanism of RITA-induced down-regulation of HH signaling, we addressed a possible involvement of the MAP kinase JNK [29,31]. Our results confirmed that suppression of this kinase by the JNK inhibitor SP600125 reverted the RITA effect on HH signaling in Daoy [Fig. 3A] and Rh36 [Fig. 3B] cells by fully rescuing the RNA levels of GLI1, PTCH1 and PTCH2. However, the expression of p53 target genes was not affected [Fig. 3A and B], highlighting the JNK independence of their response. Worth noting is that the JNK inhibitor itself slightly upregulated GLI1, GLI2, PTCH1 RNA expression in Rh36 cells [Fig. 3B].

Western blot analysis confirmed that protein levels of the 54 KDa and 46 KDa isoforms of JNK, which are dually phosphorylated at Thr183 and Tyr185 upon activation, are elevated in RITA treated (1 μM, 48hr) Daoy cells. JNK inhibition by SP600125 blocked this up-regulation and further reduced the levels of the 46 KDa isoform [Fig. 3C].

These data support the role of activated JNK in mediating the RITA effects on HH signaling.

3.4. Cytotoxic effects of RITA in Daoy and Rh36 cells

A recent study suggested that RITA exerts its effects predominantly through DNA damage, and cells with primary or acquired resistance to RITA are independent of the p53 status and display cross-resistance to DNA crosslinking compounds [26]. We hypothesized, that if the effects of RITA on HH signaling are the result of a generalized DNA damage response, then other cytotoxic agents such as doxorubicin (DXR) or oxaliplatin (OXP) could mimic the RITA-induced downregulation of GLI1/2 expression and have comparable cytotoxic effects on the cells, irrespective of their p53 status. We therefore examined the impact of different concentrations of RITA, DXR and OXP on Daoy and Rh36 cell viability.

Interestingly, in Daoy cells DXR is more toxic, reducing the fraction of viable cells by ≈ 75% already at the 0.25 μM dose, while RITA treated cells show high resistance even to the highest applied dose (10 μM), and only ≈50% reduction of viable cells at 2 μM [Fig. 4A]. However, a different scenario is observed in Rh36 cells; here RITA is more toxic, reducing cell viability by ≈ 75% already at 0.25 μM, while DXR reaches similar effects only at the 5 μM dose [Fig. 4B]. Importantly, although both Daoy and Rh36 cells are more resistant to OXP treatment, the observed dose-dependent toxicity pattern is more similar to that seen with DXR treatment [Fig. 4A and B]; the fraction of viable cells is reduced by ≈ 50% at 8 μM OXP in Daoy [Fig. 4A] and at 40 μM in Rh36 cells [Fig. 4B]. qPCR analyses confirmed that DXR did not downregulate HH signaling, since GLI1 levels were not reduced upon DXR treatment neither in Daoy nor in Rh36 cells [Figs. S4A and B]. Additionally, OXP could not mimic the RITA-induced downregulation

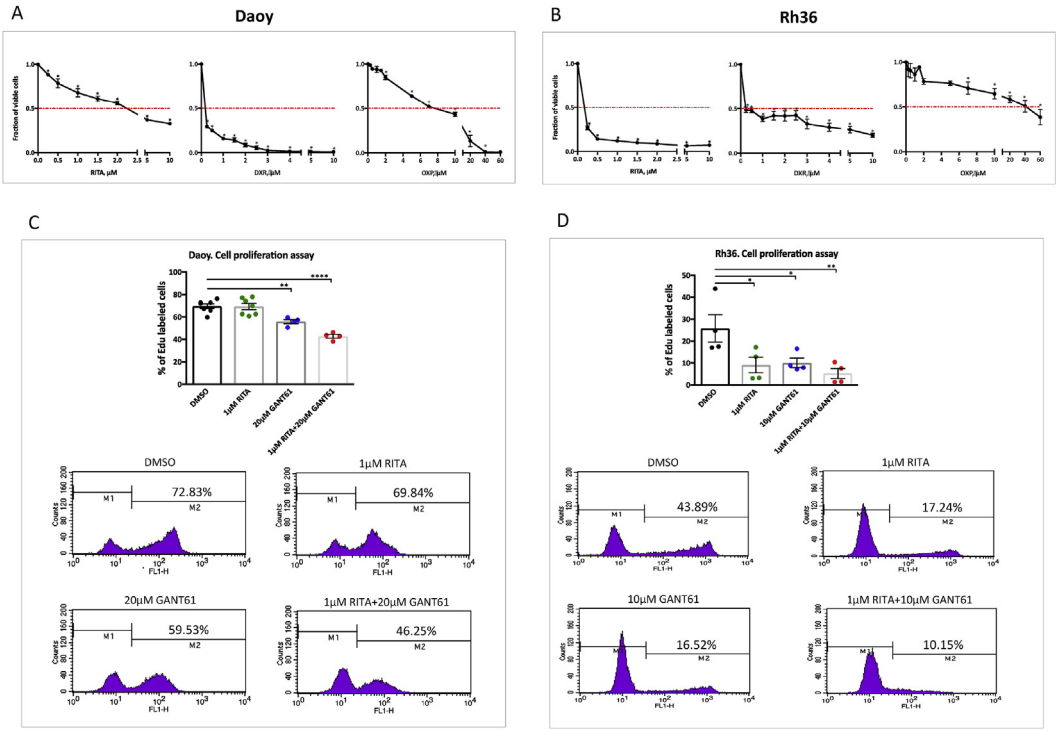

Fig. 4. *In vitro* cellular effects of RITA, doxorubicin, oxaliplatin and GANT61. **(A, B)** RITA, doxorubicin (DXR) and oxaliplatin (OXP) differentially suppress the viability of Daoy and Rh36 cells. (A) Daoy (for 48hr) and (B) Rh36 (for 24hr) cells were treated with 0.25–10 μM RITA or DXR, or 0.25–60 μM OXP. The number of viable cells (as a normalized proportion of untreated cells) was determined by the WST-1 assay. Error bars indicate the SEM of three independent biological replicates. One-way ANOVA analysis using Dunnett's multiple comparisons method was applied to determine statistically significant differences (*:$p < 0.0001$) of each treatment vs. the control. **(C, D)** Combinatorial RITA and GANT61 treatment suppresses cell proliferation *in vitro*. (C) Daoy cells were treated with 1 μM RITA, 20 μM GANT61 or a combination of both for 24hr followed by EdU incorporation for 3hr. (D) Rh36 cells were treated with 1 μM RITA, 10 μM GANT61 or a combination of both for 24hr followed by EdU incorporation for 4.5hr. (C, D) Lower panels: the percentage of cells detected by flow cytometry in representative experiments are shown in the lower panels; upper panels: bar plots summarizing grouped data from independent biological replicates. Error bars indicate the SEM of ≥4 replicates. One-way ANOVA analysis using Sidak's multiple comparisons method was applied to calculate significant differences (*:$p < 0.05$, **:$p < 0.01$, ****:$p < 0.0001$) between each treatment vs. the DMSO control.

of GLI1/2 expression [Fig. S4C]. Moreover, DXR did not elicit the JNK phosphorylation response seen with RITA, in fact, the 46 KDa isoform could not be detected following this treatment [Fig. S4D].

These observations highlight that RITA contrasts DXR and OXP in its impact on HH signaling and cytotoxicity pattern.

We have also addressed the effects of the small molecule p53-activators nutlin-3a and APR-246 on HH signaling. In Rh36 cells, nutlin-3a downregulated GLI1, but this was p53-dependent, as p53 depletion abrogated the GLI1 downregulation, while other HH target genes GLI2, PTCH1 and PTCH2 were not affected by nutlin-3a treatment [Fig. S4E]. In addition, APR-246 was not able to elicit reduction of HH signaling targets [Fig. S4F].

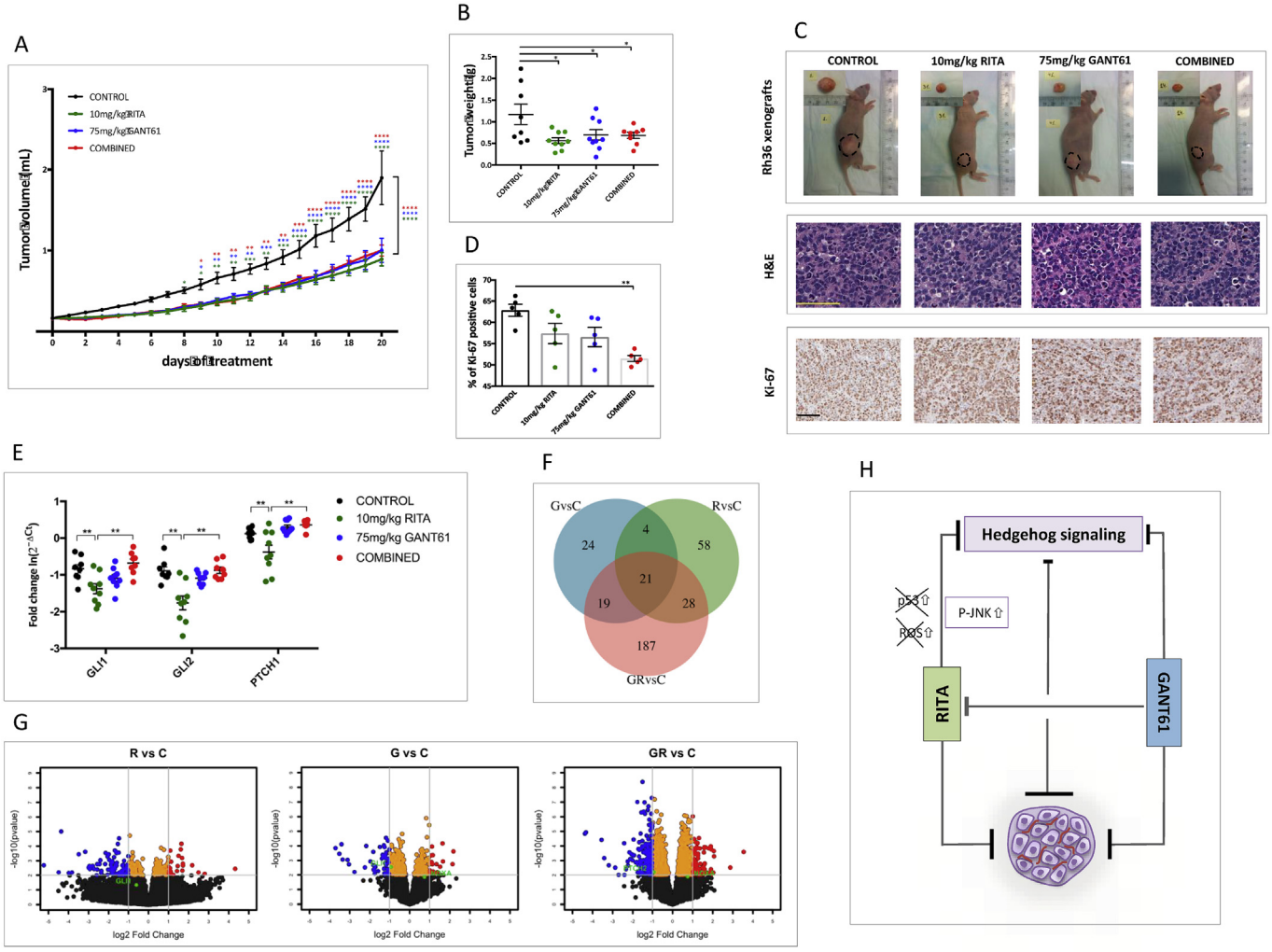

Fig. 5. Antitumor effects of RITA and GANT61 on human Rh36 cell subcutaneous xenografts. NMRI-*nu/nu* mice carrying Rh36 xenografts were treated daily for 20 days with 10 mg/kg RITA (n = 9), 75 mg/kg GANT61 (n = 9), combination of both treatments (n = 8), or received no intervention as a control group (n = 8). **(A)** Tumor volume of the four treatment groups of mice during the 20-day period. The two-way ANOVA analysis was applied to calculate significant differences of tumor growth (as volume in mLs) between each treatment vs. the control group throughout the experiment. In addition, the Dunnett's multiple comparison method (two-way ANOVA) was applied to assess significant differences (*:p < 0.05, **:p < 0.01, ***:p < 0.001, ****:p < 0.0001) between the treatment groups vs. control at each measurement. **(B)** At the end of the treatment, tumors were extracted and weighed. One-way ANOVA test was applied to assess significant differences of tumor final weight. (**C**) Representative photographs of mice sacrificed at the end-point of the experiment with corresponding tumors (Rh36 xenograft; scale on the photo), H &E stainings of tumor sections (H&E; scale bar 100 μm) and Ki-67 positive tumor sections (Ki-67; scale bar 100 μm) from control and treatment (RITA, GANT61 and combination of both drugs) groups are shown. **(D)** Percentage of Ki-67 positive cells in each treatment group; error bars indicate the SEM of 5 different tumor sections. **(E)** RNA expression of HH target genes (GLI1, GLI2, PTCH1) in tumors of control and treatment groups is presented as relative expression ln ($2^{-\Delta Ct}$) values, normalized to the housekeeping gene TBP. Error bars indicate the SEM of control (black, n = 8), RITA treated (green, n = 9), GANT61 treated (blue, n = 9) or combination treated (red, n = 8) tumors. The two-way ANOVA using Tukey's multiple comparisons method was applied to determine statistically significant differences (**:p < 0.01) between the experimental groups. **(F, G)** Illumina RNA-seq analyses of four representative tumor samples from each treatment group. (F) Venn diagram representing the 111, 68 and 255 differentially expressed genes in RITA, GANT61 and combination treated tumors relative to control (Rvs.C, Gvs.C, GRvs.C), respectively. (G) Volcano plots visualizing the differentially expressed genes in RITA, GANT61 and combination treatment relative to control (Rvs.C, Gvs.C, GRvs.C). The y-axes correspond to the mean expression value of -$\log_{10}$ (p value), and the x-axes display the $\log_2$ fold change. The black and orange dots represent gene targets whose expression levels did not reach the cut-off threshold (|$\log_2$ fold change| > 1 (i.e. 2-fold) and p < 0.01 assessed by Wald significance test); blue dots represent downregulated and red dots upregulated genes. Green dots and corresponding gene names, depict the genes from the pre-selected list of HH and p53 targets previously used in *in vitro* experiments (Supplementary file S1); milder cut-off thresholds (|$\log_2$ fold change| > 0.5 and p < 0.05 assessed by Wald significance test) were applied for this list. (**H**) Graphical diagram highlighting the inhibitory effects of RITA and GANT61 on HH signaling and xenograft tumor growth *in vivo*. Note that RITA is potent at both constraining HH signaling activity and tumor cell growth, while GANT61 has limited effects on HH signaling, but still is able to reduce tumor growth. Moreover, when administered together, GANT61 blocks RITA's downregulation of HH signaling, but still tumor growth is reduced. (For interpretation of the references to colour in this figure legend, the reader is referred to the Web version of this article.)

3.5. RITA and the GLI inhibitor GANT61 co-treatments suppress cell proliferation and enhance apoptosis in Daoy and Rh36 cells

To further examine the relevance of RITA treatment for HH signaling-dependent tumor cells, we investigated the effects of RITA on cell proliferation and apoptosis assays, and the impact of co-administration with the GLI inhibitor GANT61. Our results indicate that RITA and GANT61 co-treatment sensitizes Daoy cells, as it resulted in a more pronounced reduction of cell proliferation [Fig. 4C] and an increase of apoptosis [Figs. S5A and B]. However, in this cellular context the GANT61 concentration was increased to 20 μM for detection of these effects [Fig. S5C]. In fact, GANT61, in contrast to RITA, has little impact on HH signaling in Daoy and Rh36 cells [Fig. S5D-F; S6E], and it is only in the context of HH signaling activation that GANT61 can elicit a pronounced downregulation of HH signaling [Fig. S5E].

Additionally, RITA and GANT61 co-treatment exhibits enhanced effects in suppressing cell proliferation in Rh36 [Fig. 4D].

These results suggest that RITA and GANT61 co-administration may have advantages in inhibiting tumor cell growth.

3.6. Antitumor effects of RITA and GANT61 on Rh36 xenografts in nude mice

To examine the *in vivo* effects of RITA and GANT61, we generated Rh36 cell derived subcutaneous xenograft tumors in nude mice. After formation of palpable tumors at ≥0.150 mL volume, mice received daily intraperitoneal injections of 10 mg/kg RITA, oral gavage administrations of 75 mg/kg GANT61, combination of both treatments or no intervention (control) for 20 days [Fig. 5; Fig. S7]. In comparison with the control group, both RITA and GANT61 treatments significantly and to a similar extent suppressed tumor growth (measured as tumor volume) starting from treatment day 9 and persisting until the end day of treatment [Fig. 5A]. Combined administration of RITA and GANT61 did not enhance the tumor-suppressing effect of each drug, assessed as tumor volume during 20 days of treatment [Fig. 5A], or tumor weight at the end of treatment [Fig. 5B]. Nevertheless, compared to RITA and GANT61, the combination treatment minimized the tumor volume variation within this group, especially throughout days 10–20 [Fig. S7A]. Comparison of H&E stained tumor sections suggested similar morphology between tumors of the control and treatment groups, with highly proliferative cell patterns and necrotic patches throughout the tumors [Fig. 5C]. The fraction of Ki-67 positively stained cells was significantly decreased only in the combination treatment [Fig. 5D].

Remarkably, qPCR analyses of all tumor samples demonstrated that although the mRNA expression of the typical HH target genes GLI1, GLI2 and PTCH1 was downregulated following RITA administration, this was hardly observed with GANT61 and completely eliminated by the combination treatment [Fig. 5E]. Thus, GANT61 can abrogate the HH signaling downregulation elicited by RITA.

Moreover, in Daoy cell xenografts of nude mice, 75 mg/kg GANT61 oral gavage administration did not result in reduction of tumor growth [Figs. S6A-D] or inhibition of HH signaling target gene expression [Fig. S6E].

3.7. RNA-seq analysis of Rh36 xenografts

Next, RNA-seq analyses was performed on 4 tumor samples from each of the Rh36 xenograft treatment group [Supplementary Table 2]. Differentially expressed genes were defined as having at least 2-fold change compared to control ($|\log_2 \text{foldchange}| > 1$, $p < 0.01$) and are presented in the Venn diagram [Fig. 5F] and the Volcano plots [Fig. 5G; Fig. S7C], [Supplementary file S1]. Additionally, a pre-selected list of 12 genes used in the *in vitro* qPCR experiments [Supplementary file S1] was interrogated with more relaxed criteria ($|\log_2 \text{foldchange}| > 0.5$, $p < 0.05$). Notably, compared to the control group C, the number of differentially regulated genes in the combination treatment GR (255 genes) was about twice higher than in the RITA treatment group R (111 genes) and about three times higher than in the GANT61 treatment group G (68 genes). In addition, the number of uniquely differentially expressed genes in the GR vs. C comparison was about three times higher than in the R vs. C and about eight times higher than G vs. C comparison [Fig. 5F]. The RNA-seq analyses confirmed a significant downregulation of GLI1 only in the RITA and GANT61 treated xenografts, reaching ≈50% compared to control, inline with mRNA expression data of the GLI1 qPCR amplicons [Fig. S7B]. The only observed significant downregulation of a HH target in the combination group was that of PTCH2 [Fig. 5G: GR vs. C]. Consistent with the broader gene regulation seen in the combination treatment, Gene Ontology (GO) enrichment analyses resulted in more GO terms, including terms associated with cell growth, in the GR vs. C gene list relative to the R vs. C or the G vs. C lists [Figs. S8A–D], [Supplementary files S2 [Rvs.C]; S3 [Gvs.C]; S4 [GRvs.C]]. KEGG pathway enrichment analyses also highlighted that the GR vs. C gene list results in 6 significantly enriched pathways, including the MAPK, PI3K-Akt, Rap1 and TGF-beta signaling pathways, while the G vs. C list in only MAPK and the R vs. C list in none [Fig. S8E], [Supplementary files S2 [Rvs.C]; S3 [Gvs.C]; S4 [GRvs.C]].

Taken together, these results suggest that the combination treatment elicits a broader response compared to individual treatments, and this may rationalize the observed reduction of tumor growth, even though HH signaling is not appreciably downregulated.

4. Discussion

Defective regulation and inappropriate activation of the HH signaling pathway is implicated in many cancers. SMO targeting inhibitors were the first to enter clinical trials, however complications with acquired resistance and toxicity, also exemplified in preclinical studies of various tumor models, demonstrated that inhibition of SMO alone does not provide long-term efficacy in constraining tumor progression [43–46]. Additionally, dysregulation of other pathways that crosstalk with HH signaling components, including the tumor suppressor p53, can also contribute to tumor maintenance and resistance. Hence, combinatorial treatments and/or “switching off” the HH signal transduction cascade by direct inhibition of the terminal effectors of the pathway, the GLI factors, may overcome both SMO and “non canonical” HH pathway-driven resistance.

In this study we demonstrate that the small molecule RITA downregulates HH signaling irrespective of the p53 status (wild-type or mutant) in the cells or p53 depletion via siRNAs. In three different cellular contexts, Daoy MB, Rh36 RMS and MCF7 breast cancer cells, RITA was capable to downregulate RNA expression of typical HH target genes (GLI1, GLI2, PTCH1, PTCH2) [Fig. 1A; Figs. S1A and B] irrespective of p53 depletion. We also provide evidence that the RITA effects are apparently elicited downstream of SMO, since depletion of SMO did not confer major changes in the response of the HH target genes [Fig. 1A; Fig. S1A].

Although since its discovery RITA (NSC652287) [20,47] has generally been considered to exert its tumor suppressive effects in a p53-dependent manner [22–24,31,48], in recent years the p53-dependence of the RITA effects was debated, as several studies highlighted RITA-mediated effects without any obvious dependency on the cells' p53 status [26–28], questioning even its selective binding to the p53 protein [25]. In fact, our studies show that in Daoy cells, the p53 protein levels are unchanged upon RITA treatment [Fig. 1C], and the p53 target gene expression levels show only small and sometimes rather inconsistent changes, which in addition are not dependent on p53 depletion [Fig. 1A; Fig. 2A and B; Fig. 3A]. These findings further support the notion that RITA can elicit p53-independent effects.

Since ROS-dependent JNK activation has been suggested as a possible mechanism of RITA action [31,32], we studied its potential involvement in the observed HH signaling downregulation. First, ROS

accumulation was prevented by different antioxidants (resveratrol and NAC) and second, JNK activity was inhibited by the small molecule SP600125. We found that both resveratrol and NAC were mostly ineffective in reverting the RITA mediated effects on HH signaling gene expression in both Daoy and Rh36 cells [Fig. 2A and B; Figs. S2A–F]. However, JNK inhibition fully rescued the RITA effects [Fig. 3A and B]. Interestingly, the JNK inhibitor did not revert the effect of RITA on p53 target gene expression neither in Daoy [Fig. 3A] nor in Rh36 cells [Fig. 3B], further supporting the claim that the impact of RITA on HH signaling is p53 independent. In fact, these data are in agreement with a dual mechanism of RITA action, a JNK-independent p53 response and a JNK-dependent HH signaling response. Western blot analysis in Daoy cells confirmed that the protein levels of the 54 KDa and 46 KDa JNK isoforms are elevated by activating phosphorylation upon RITA treatment [Fig. 3C].

Recently, a plausible scenario underlying the RITA effects was put forward, suggesting that cells develop resistance to RITA independent of the p53 status, with this resistance not mediated by p53 mutations, but rather by defects in the DNA damage signaling network, which can be induced via both p53-dependent and p53-independent mechanisms [26]. To address this possibility, the cell viability and/or the GLI1/GLI2 RNA expression response of two additional cytotoxic agents (DXR and OXP) was compared to that of RITA. Interestingly, compared to Daoy cells [Fig. 4A,C; Figs. S5A–C], Rh36 cells were much more sensitive to RITA [Fig. 4B, D]. Yet, these two cell lines responded with a similar pattern to both DXR and OXP treatments, with Daoy cells being more sensitive to OXP and DXR. The higher sensitivity of Rh36 cells to RITA treatment might be due to the potentiality of wild-type p53 in inducing a p53 dependent response. In fact, this scenario is consistent with the fact that RITA is a much better inducer of p53 targets (NOXA and BCL2) in wild-type p53 Rh36 cells [Figs. S2A,B,E,F], compared to mutant p53 Daoy cells [Fig. 2A and B; S2C,D]. Further evidence on the differential impact of these drugs is provided by qPCR analyses, which confirmed that DXR does not downregulate GLI1 levels [Figs. S4A and B], in line with a previously reported study [49], and OXP could not mimic the RITA-induced downregulation of GLI1/2 expression [Fig. S4C]. In this context, quite revealing is the finding that DXR was not able to elicit the JNK phosphorylation response observed by RITA [Fig. 3C], with the 46 KDa isoform levels becoming undetectable following this treatment [Fig. S4D], similarly to what is seen when the JNK inhibitor impedes the RITA upregulation of phospho-JNK. Taken together, these results provide evidence that compared to the DNA damaging agents DXR and OXP, RITA has distinct cytotoxic readouts and differential impact on HH signaling. Worth noting is that two known p53 activating drugs, nutlin-3a and APR-246 (PRIMA-1Met) [50], were rather ineffective in downregulating HH signaling target genes [Figs. S4E and F], again highlighting the distinct action of RITA on HH signaling.

Although in *in vitro* analyses GANT61 sensitized Daoy cells to RITA treatment, this was not fully reflected in the *in vivo* xenograft studies in nude mice, as the combinatorial treatment elicited a comparable reduction of tumor growth. However, the dual drug administration reduced within-group variation, seen in volume measurements throughout the experiment [Fig. S7A], and downregulated tumor cell proliferation [Fig. 5D]. In fact, in the Rh36 subcutaneous xenografts, the observed tumor suppressive effects were correlated with HH signaling downregulation, primarily with RITA and to a lesser extent with GANT61 administration. Moreover, in the combinatorial treatment, GANT61 apparently blocked the suppressive effects of RITA on HH targets [Fig. 5E,G; Fig. S7B]. Consequently, our findings pinpoint to variable modes of RITA and GANT61 action, with the combinatorial treatment blocking the RITA effects and eliciting a broader response, exemplified by the GO and KEGG pathway enrichment analyses [Fig. S8].

In conclusion, our data demonstrate that RITA reduces HH signaling irrespective of p53 in medulloblastoma and rhabdomyosarcoma cells. Surprisingly, GANT61 is not as effective as RITA in downregulating HH signaling, with the dual drug administration almost completely blocking the HH signaling response *in vivo*, suggesting a certain antagonism of the two drugs.

Conflicts of interest

The other authors declare no potential conflicts of interest.

Acknowledgements

This study was funded by the Swedish Cancer Society and the Swedish Childhood Cancer Foundation. A.A. was supported by the Karolinska Institutet Doctoral (KID) funding program and Y.D. by the China Scholarship Council. Rune Toftgård and Vladimir Bykov are acknowledged for helpful discussions. Raoul Kuiper and Agneta B. Andersson are acknowledged for their help in immunohistochemistry analyses. The authors also would like to thank the core facility at NEO, BEA, Bioinformatics and Expression analysis, which is supported by the board of research at the Karolinska Institute and the research committee at the Karolinska Hospital.

GS is a founder of Aprea AB.

Appendix A. Supplementary data

Supplementary data to this article can be found online at https://doi.org/10.1016/j.canlet.2018.11.005.

References

[1] F. Aberger, I.A.A. Ruiz, Context-dependent signal integration by the GLI code: the oncogenic load, pathways, modifiers and implications for cancer therapy, Semin. Cell Dev. Biol. 33 (2014) 93–104.
[2] J. Briscoe, P.P. Therond, The mechanisms of Hedgehog signalling and its roles in development and disease, Nat. Rev. Mol. Cell Biol. 14 (2013) 416–429.
[3] P.W. Ingham, A.P. McMahon, Hedgehog signaling in animal development: paradigms and principles, Genes Dev. 15 (2001) 3059–3087.
[4] S. Teglund, R. Toftgård, Hedgehog beyond medulloblastoma and basal cell carcinoma, Biochim. Biophys. Acta 1805 (2010) 181–208.
[5] D. Amakye, Z. Jagani, M. Dorsch, Unraveling the therapeutic potential of the Hedgehog pathway in cancer, Nat. Med. 19 (2013) 1410–1422.
[6] J.M. Ng, T. Curran, The Hedgehog's tale: developing strategies for targeting cancer, Nat. Rev. Canc. 11 (2011) 493–501.
[7] J.M. Rusert, X. Wu, C.G. Eberhart, M.D. Taylor, R.J. Wechsler-Reya, SnapShot: medulloblastoma, Cancer Cell 26 (2014) 940 e941.
[8] A. Uhmann, U. Ferch, R. Bauer, S. Tauber, Z. Arziman, C. Chen, B. Hemmerlein, L. Wojnowski, H. Hahn, A model for PTCH1/Ptch1-associated tumors comprising mutational inactivation and gene silencing, Int. J. Oncol. 27 (2005) 1567–1575.
[9] W.M. Roberts, E.C. Douglass, S.C. Peiper, P.J. Houghton, A.T. Look, Amplification of the gli gene in childhood sarcomas, Cancer Res. 49 (1989) 5407–5413.
[10] D.O. Brien, A.G. Jacob, S.J. Qualman, D.S. Chandler, Advances in pediatric rhabdomyosarcoma characterization and disease model development, Histol. Histopathol. 27 (2012) 13–22.
[11] C. Wetmore, D.E. Eberhart, T. Curran, Loss of p53 but not ARF accelerates medulloblastoma in mice heterozygous for patched, Cancer Res. 61 (2001) 513–516.
[12] R.L. Carpenter, H.W. Lo, Hedgehog pathway and GLI1 isoforms in human cancer, Discov. Med. 13 (2012) 105–113.
[13] M. Kasper, G. Regl, A.M. Frischauf, F. Aberger, GLI transcription factors: mediators of oncogenic Hedgehog signalling, Eur. J. Canc. 42 (2006) 437–445.
[14] M. Lauth, A. Bergstrom, T. Shimokawa, R. Toftgård, Inhibition of GLI-mediated transcription and tumor cell growth by small-molecule antagonists, Proc. Natl. Acad. Sci. U. S. A. 104 (2007) 8455–8460.
[15] U. Tostar, R. Toftgård, P.G. Zaphiropoulos, T. Shimokawa, Reduction of human embryonal rhabdomyosarcoma tumor growth by inhibition of the hedgehog signaling pathway, Genes Cancer 1 (2010) 941–951.
[16] M. Wickström, C. Dyberg, T. Shimokawa, J. Milosevic, N. Baryawno, O.M. Fuskevag, R. Larsson, P. Kogner, P.G. Zaphiropoulos, J.I. Johnsen, Targeting the hedgehog signal transduction pathway at the level of GLI inhibits neuroblastoma cell growth in vitro and in vivo, Int. J. Canc. 132 (2013) 1516–1524.
[17] J.S. Fu, M. Rodova, S.K. Roy, S. Shankar, R.K. Srivastava, GANT-61 inhibits pancreatic cancer stem cell growth in vitro and in NOD/SCID/IL2R gamma null mice xenograft, Cancer Res. 73 (2013).
[18] L.L. Huang, V. Walter, D.N. Hayes, M. Onaitis, Hedgehog-GLI signaling inhibition suppresses tumor growth in squamous lung cancer, Clin. Canc. Res. 20 (2014) 1566–1575.
[19] Y. Wang, C. Han, L. Lu, S. Magliato, T. Wu, Hedgehog signaling pathway regulates autophagy in human hepatocellular carcinoma cells, Hepatology 58 (2013) 995–1010.

[20] M.I. Rivera, S.F. Stinson, D.T. Vistica, J.L. Jorden, S. Kenney, E.A. Sausville, Selective toxicity of the tricyclic thiophene NSC652287 in renal carcinoma cell lines - differential accumulation and metabolism, Biochem. Pharmacol. 57 (1999) 1283–1295.
[21] M. Burmakin, Y. Shi, E. Hedstrom, P. Kogner, G. Selivanova, Dual targeting of wild-type and mutant p53 by small molecule RITA results in the inhibition of N-Myc and key survival oncogenes and kills neuroblastoma cells in vivo and in vitro, Clin. Canc. Res. 19 (2013) 5092–5103.
[22] F. Nikulenkov, C. Spinnler, H. Li, C. Tonelli, Y. Shi, M. Turunen, T. Kivioja, I. Ignatiev, A. Kel, J. Taipale, G. Selivanova, Insights into p53 transcriptional function via genome-wide chromatin occupancy and gene expression analysis, Cell Death Differ. 19 (2012) 1992–2002.
[23] V.V. Grinkevich, F. Nikulenkov, Y. Shi, M. Enge, W. Bao, A. Maljukova, A. Gluch, A. Kel, O. Sangfelt, G. Selivanova, Ablation of key oncogenic pathways by RITA-reactivated p53 is required for efficient apoptosis, Cancer Cell 15 (2009) 441–453.
[24] N. Issaeva, P. Bozko, M. Enge, M. Protopopova, L.G. Verhoef, M. Masucci, A. Pramanik, G. Selivanova, Small molecule RITA binds to p53, blocks p53-HDM-2 interaction and activates p53 function in tumors, Nat. Med. 10 (2004) 1321–1328.
[25] M. Krajewski, P. Ozdowy, L. D'Silva, U. Rothweiler, T.A. Holak, NMR indicates that the small molecule RITA does not block p53-MDM2 binding in vitro, Nat. Med. 11 (2005) 1135–1136 author reply 1136-1137.
[26] M. Wanzel, J.B. Vischedyk, M.P. Gittler, N. Gremke, J.R. Seiz, M. Hefter, M. Noack, R. Savai, M. Mernberger, J.P. Charles, J. Schneikert, A.C. Bretz, A. Nist, T. Stiewe, CRISPR-Cas9-based target validation for p53-reactivating model compounds, Nat. Chem. Biol. 12 (2016) 22–28.
[27] H.C. Chuang, L.P. Yang, A.L. Fitzgerald, A. Osman, S.H. Woo, J.N. Myers, H.D. Skinner, The p53-reactivating small molecule RITA induces senescence in head and neck cancer cells, PLoS One 9 (2014) e104821.
[28] A. Weilbacher, M. Gutekunst, M. Oren, W.E. Aulitzky, H. van der Kuip, RITA can induce cell death in p53-defective cells independently of p53 function via activation of JNK/SAPK and p38, Cell Death Dis. 5 (2014) e1318.
[29] M.N. Saha, H. Jiang, Y. Yang, X. Zhu, X. Wang, A.D. Schimmer, L. Qiu, H. Chang, Targeting p53 via JNK pathway: a novel role of RITA for apoptotic signaling in multiple myeloma, PLoS One 7 (2012) e30215.
[30] R.J. Davis, Signal transduction by the JNK group of MAP kinases, Cell 103 (2000) 239–252.
[31] Y. Shi, F. Nikulenkov, J. Zawacka-Pankau, H. Li, R. Gabdoulline, J. Xu, S. Eriksson, E. Hedstrom, N. Issaeva, A. Kel, E.S. Arner, G. Selivanova, ROS-dependent activation of JNK converts p53 into an efficient inhibitor of oncogenes leading to robust apoptosis, Cell Death Differ. 21 (2014) 612–623.
[32] E. Hedström, S. Eriksson, J. Zawacka-Pankau, E.S. Arner, G. Selivanova, p53-dependent inhibition of TrxR1 contributes to the tumor-specific induction of apoptosis by RITA, Cell Cycle 8 (2009) 3584–3591.
[33] L. Amable, E. Gavin, K. Kudo, E. Meng, R.P. Rocconi, L.A. Shevde, E. Reed, GLI1 upregulates C-JUN through a specific 130-kDa isoform, Int. J. Oncol. 44 (2014) 655–661.
[34] T. Shiohama, K. Fujii, H. Uchikawa, T. Takatani, H. Mizuochi, Y. Kohno, Oxidative stress-induced JNK1 phosphorylation inhibits hedgehog signalling and osteoblast differentiation, Cell Biol. Int. Rep. 21 (2014) 53–62.
[35] T.C. Whisenant, D.T. Ho, R.W. Benz, J.S. Rogers, R.M. Kaake, E.A. Gordon, L. Huang, P. Baldi, L. Bardwell, Computational prediction and experimental verification of new MAP kinase docking sites and substrates including Gli transcription factors, PLoS Comput. Biol. 6 (2010).
[36] S. Laner-Plamberger, A. Kaser, M. Paulischta, C. Hauser-Kronberger, T. Eichberger, A.M. Frischauf, Cooperation between GLI and JUN enhances transcription of JUN and selected GLI target genes, Oncogene 28 (2009) 1639–1651.
[37] A.K. Metzger, V.C. Sheffield, G. Duyk, L. Daneshvar, M.S. Edwards, P.H. Cogen, Identification of a germ-line mutation in the p53 gene in a patient with an intracranial ependymoma, Proc. Natl. Acad. Sci. U. S. A. 88 (1991) 7825–7829.
[38] R.L. Saylors 3rd, D. Sidransky, H.S. Friedman, S.H. Bigner, D.D. Bigner, B. Vogelstein, G.M. Brodeur, Infrequent p53 gene mutations in medulloblastomas, Cancer Res. 51 (1991) 4721–4723.
[39] T. Shimokawa, M.F. Rahman, U. Tostar, E. Sonkoly, M. Stahle, A. Pivarcsi, R. Palaniswamy, P.G. Zaphiropoulos, RNA editing of the GLI1 transcription factor modulates the output of Hedgehog signaling, RNA Biol. 10 (2013) 321–333.
[40] V.E. Villegas, M.F. Rahman, M.G. Fernandez-Barrena, Y. Diao, E. Liapi, E. Sonkoly, M. Stahle, A. Pivarcsi, L. Annaratone, A. Sapino, S. Ramirez Clavijo, T.R. Burglin, T. Shimokawa, S. Ramachandran, P. Kapranov, M.E. Fernandez-Zapico, P.G. Zaphiropoulos, Identification of novel non-coding RNA-based negative feedback regulating the expression of the oncogenic transcription factor GLI1, Mol. Oncol. 8 (2014) 912–926.
[41] Y. Diao, A. Azatyan, M.F. Rahman, C. Zhao, J. Zhu, K. Dahlman-Wright, P.G. Zaphiropoulos, Blockade of the Hedgehog pathway downregulates estrogen receptor alpha signaling in breast cancer cells, Oncotarget 7 (2016) 71580–71593.
[42] K.J. Livak, T.D. Schmittgen, Analysis of relative gene expression data using real-time quantitative PCR and the 2(-Delta Delta C(T)) Method, Methods 25 (2001) 402–408.
[43] H.J. Sharpe, G. Pau, G.J. Dijkgraaf, N. Basset-Seguin, Z. Modrusan, T. Januario, V. Tsui, A.B. Durham, A.A. Dlugosz, P.M. Haverty, R. Bourgon, J.Y. Tang, K.Y. Sarin, L. Dirix, D.C. Fisher, C.M. Rudin, H. Sofen, M.R. Migden, R.L. Yauch, F.J. de Sauvage, Genomic analysis of smoothened inhibitor resistance in basal cell carcinoma, Cancer Cell 27 (2015) 327–341.
[44] J. Kim, B.T. Aftab, J.Y. Tang, D. Kim, A.H. Lee, M. Rezaee, J. Kim, B. Chen, E.M. King, A. Borodovsky, G.J. Riggins, E.H. Epstein Jr., P.A. Beachy, C.M. Rudin, Itraconazole and arsenic trioxide inhibit Hedgehog pathway activation and tumor growth associated with acquired resistance to smoothened antagonists, Cancer Cell 23 (2013) 23–34.
[45] M. Kasper, R. Toftgård, Smoothing out drug resistance, Cancer Cell 23 (2013) 3–5.
[46] R.L. Yauch, G.J. Dijkgraaf, B. Alicke, T. Januario, C.P. Ahn, T. Holcomb, K. Pujara, J. Stinson, C.A. Callahan, T. Tang, J.F. Bazan, Z. Kan, S. Seshagiri, C.L. Hann, S.E. Gould, J.A. Low, C.M. Rudin, F.J. de Sauvage, Smoothened mutation confers resistance to a Hedgehog pathway inhibitor in medulloblastoma, Science 326 (2009) 572–574.
[47] W. Nieves-Neira, M.I. Rivera, G. Kohlhagen, M.L. Hursey, P. Pourquier, E.A. Sausville, Y. Pommier, DNA protein cross-links produced by NSC 652287, a novel thiophene derivative active against human renal cancer cells, Mol. Pharmacol. 56 (1999) 478–484.
[48] C.Y. Zhao, V.V. Grinkevich, F. Nikulenkov, W. Bao, G. Selivanova, Rescue of the apoptotic-inducing function of mutant p53 by small molecule RITA, Cell Cycle 9 (2010) 1847–1855.
[49] D. Mazza, P. Infante, V. Colicchia, A. Greco, R. Alfonsi, M. Siler, L. Antonucci, A. Po, E. De Smaele, E. Ferretti, C. Capalbo, D. Bellavia, G. Canettieri, G. Giannini, I. Screpanti, A. Gulino, L. Di Marcotullio, PCAF ubiquitin ligase activity inhibits Hedgehog/Gli1 signaling in p53-dependent response to genotoxic stress, Cell Death Differ. 20 (2013) 1688–1697.
[50] V.J.N. Bykov, S.E. Eriksson, J. Bianchi, K.G. Wiman, Targeting mutant p53 for efficient cancer therapy, Nat. Rev. Canc. 18 (2018) 89–102.